Automated DeepLabV3+ based model for left ventricle segmentation on short-axis late gadolinium enhancement-magnetic cardiac resonance imaging images

Dayang Suhaida Awang Damit[1], Siti Noraini Sulaiman[1,2,5], Muhammad Khusairi Osman[1], Noor Khairiah A. Karim[3,4], Samsul Setumin[1]

[1]Electrical Engineering Studies, College of Engineering, Universiti Teknologi MARA Cawangan Pulau Pinang, Permatang Pauh Campus, Pulau Pinang, Malaysia
[2]Integrative Pharmacogenomics Institute (iPROMISE), Universiti Teknologi MARA, Puncak Alam Campus, Selangor, Malaysia
[3]Department of Biomedical Imaging, Advanced Medical and Dental Institute, Universiti Sains Malaysia-Bertam, Pulau Pinang, Malaysia
[4]Heart Failure Research Initiative, Advanced Medical and Dental Institute, Universiti Sains Malaysia-Bertam, Pulau Pinang, Malaysia
[5]Advanced Rehabilitation Engineering in Diagnostic and Monitoring Research Group (AREDiM), Electrical Engineering Studies, College of Engineering, Universiti Teknologi MARA Cawangan Pulau Pinang, Permatang Pauh Campus, Pulau Pinang, Malaysia

Article Info

ABSTRACT

Accurate segmentation of myocardial scar tissue on late gadolinium enhancement-magnetic cardiac resonance imaging (LGE-CMR) is exceptionally vital for clinical applications, enabling precise diagnosis and effective treatment of various cardiac diseases, such as myocardial infarction and cardiomyopathies. However, the ventricle (LV) variations in the size and shape, artifacts, and image resolution of LGE-CMR has made automatic segmentation of myocardial scar tissue more challenging. While many existing approaches delineate the LV myocardium region using multi-modal segmentation, these models may be computationally complex and suffer from misalignment. Therefore, this study proposed an automatic dual-stage DeepLabV3+ based approach tailored for myocardial scar segmentation on short-axis LGE-MRI exclusively. To segment myocardial scar tissue, the second stage employs the segmented LV chamber from the previous stage. The encoder part of the framework utilizes a MobileNetV2 and ResNet50 backbone for the first and second segmentation, respectively, aiming for optimal resolution of feature maps. Both stages tailor an improved Atrous Spatial Pyramid Pooling module in the DeepLabV3+ model with fine-tuned dilated atrous rates to effectively extract the LV chamber and myocardial scar from the complex LGE-MRI background. Based on the results, the proposed dual-stage network recorded an outstanding segmentation performance, with mean Dice score of 96.02% for LV chamber segmentation and 68.01% for scar tissue extraction.

Corresponding Author:

Siti Noraini Sulaiman
Electrical Engineering Studies, College of Engineering, Universiti Teknologi MARA
Puncak Alam Campus, Bandar Puncak Alam, Puncak Alam, Selangor, Malaysia
Email: sitinoraini@uitm.edu.my

1. INTRODUCTION

Over the past decades, ischemic heart diseases have steadily manifested as a leading cause of death in various countries [1]–[3]. The presence of an infarcted tissue, known as a myocardial scar, is a major indicator of ischemic heart disease and can be accurately diagnosed using magnetic resonance imaging (MRI). The late gadolinium enhancement-cardiac magnetic resonance (LGE-CMR) is considered a gold

standard technique to evaluate the characteristics of infarcted tissue [4], [5], where fibrotic and scarring regions signify an early or current myocardium infarction episode [6]. Nevertheless, LGE-CMR image analysis is a laborious task that requires trained professionals' expertise to accurately delineate cardiac structures, including the left ventricle and scar regions, within the acquired images to quantify the scar transmurality precisely. As the demand for cardiac MRI analysis persistently grows [7], [8], medical experts such as radiologists and physicians are burdened with the overwhelming pressure to precisely analyze stacks of MR images via a manual approach in a timely manner. Therefore, developing an automated segmentation model is essential to assist the increasing interest in medical image analysis.

Recent studies have demonstrated the effective application of convolution neural networks (CNNs) in segmenting medical images across various fields such as breast cancer [9], [10] and lung segmentation [11]. Precise segmentation of the LV region, particularly areas containing scar tissue, provides a robust foundation for precise subsequent segmentation of myocardial scar tissue. A comprehensive review of deep learning for cardiac image segmentation by Chen *et al.* [12] revealed that the majority of studies in contemporary cardiovascular imaging research employing other modality on short-axis MRI data such as cine, T2-weighed, and balanced-steady state free precession (bSSFP) CMR, for delineate the LV region [13]–[16] as a predominant strategy, diverging from direct segmentation exclusively on late gadolinium enhancement (LGE-CMR) images. This is due to the segmentation of LV region from LGE-CMR images is more challenging than other modalities due to the significantly enhanced visual of the scar tissues while the signal from healthy tissues is attenuated. Furthermore, the shape and size of the LV significantly vary among patients and even from the same patient at different time points increase the difficulty of accurately identifying its boundaries. However, the result of their multimode models may need to be revised to prevent misaligned registration between LGE and other modalities, and the model may require high computational resources.

Several studies have attempted direct scar segmentation from LGE-CMR images. While Moccia *et al.* [17] demonstrated the first few networks using fully convolutional neural networks (FCNNs), their scar segmentation accuracy remained relatively low. Building upon this, Chen *et al.* [18] employed a U-Net model, achieving improved results. However, their analysis was restricted to the middle image slices, disregarding crucial basal and apical regions. This work addresses the limitation of previous research by incorporating all cardiac image slices, from epicardial to basal, aiming to achieve improved end-to-end scar segmentation accuracy on LGE-CMR images. We propose a new automatic dual-stage DeepLabV3+ based model and evaluate its performance compared to the original DeepLabV3+ model architecture on the same dataset to demonstrate the effectiveness of the proposed framework. The subsequent sections of this paper are structured as follows: Section 2 offers details regarding the dataset and the proposed dual-stage segmentation model. The results of the experiments are presented in Section 3. Finally, Section 4 draws insightful conclusions based on the findings.

2. RESEARCH METHOD

2.1. Dataset preparation

The dataset for this study was acquired from the Advanced Medical and Dental Institute (AMDI), Universiti Sains Malaysia (USM), Bertam, Pulau Pinang. All images were provided in digital imaging and communications in medicine (DICOM) format before being anonymized and converted into bitmap image file (bmp) format. For this preliminary study phase, we assembled a dataset of 178 LGE-CMR slices randomly from patients who underwent LGE-CMR scan, comprising 117 from pathological cases and 61 from normal cases. Each image's ground truth was manually segmented by an experienced radiologist, as shown in Figure 1. Figure 1(a) shows an example of LGE-CMR image, the corresponding manual segmentation of the left ventricle (LV) chamber and the infarcted scar tissue by an experienced radiologist is shown in Figure 1(b) and Figure 1(c), respectively. To increase the diversity and variability of the pathological slices, we applied geometric transformations such as rotations, resulting in a total of 412 augmented images. Of these, 60% were used for training, 20% for validation, and the remaining 20% were held for separate testing to ensure unbiased performance evaluation.

2.2. The proposed dual-stage segmentation model

This study proposed a new automatic dual-stage segmentation model built upon DeepLabV3+ as the base model to assist radiologists in segmenting scar tissue for accurate myocardial infarction assessment using LGE-MRI. This modification approach assists the segmentation of scar tissues within variation of LV region (LV chamber) from intricate backgrounds that frequently interfere with the segmentation process. DeepLabV3+ introduced by Chen *et al.* [19] is an advanced variant of semantic segmentation network, consisting of the backbone architecture as a feature extractor, the atrous spatial pyramid pooling (ASPP) module, and the decoder. The ASPP module is a vital component in DeepLabV3+ that captures multi-scale

contextual information. The original module comprises four convolutional layers, including a 1x1 dilation convolution, three 3x3 dilation convolutions with different atrous rates of 1, 6, 12, and 18, and a single global average-pooling layer. Building upon the successful DeepLabV3+ architecture, this study proposes an enhancement model as illustrated in Figure 2, employing depthwise separable convolutions (DSConv), at ASPP modules to effectively segment the anatomical variations of LV chambers and scar segmentation in LGE-CMR images. Figure 2 illustrates the encoder-decoder structure of the proposed model. The improved ASPP module used in both the LV chamber segmentation model and the scar segmentation model is shown for comparison in 2(a) and 2(b). The first stage, LV chamber segmentation, plays a crucial role in isolating the target area where infarcted scar tissue is likely present. We named this model DeepLab Tailor to LV (DLT-LV). Depthwise separable convolutions are known for their efficiency in reducing computational requirements compared to standard convolutions. The DSConv module, depthwise convolution followed by pointwise convolution layer. Depthwise convolution applies a 3×3 kernel convolution to each individual input channel, while pointwise convolution creates a linear combination of the output feature maps resulting from depthwise convolution, integrating cross-channel information [20]. Batch normalization followed by rectified linear unit (ReLU) activation function was incorporated after each 1×1 pointwise convolution operation to enhance the output quality compared to the output obtained solely from the convolutional layer. In addition, we expand the module by introducing a supplementary DSConv unit only in DLT-LV, resulting in a comprehensive assembly of five DSConv modules operating in parallel with fine-tuning the dilated convolution rates of 1, 2, 6, 12, and 18 to capture sufficient spatial details of this region of interest effectively. For the second stage model, modified ASPP consist of four DSConv modules utilized lower atrous rates of 1, 2, 3, and 3 for scar tissue segmentation, which smaller atrous dilation rates facilitate extracting features from feature maps characterized by a smaller scale. In the decoder part, features from the ASPP module were upsampled by a factor of 4 using bilinear interpolation. In addition, low-level features from the backbone architecture were subjected to a 1×1 convolution before being concatenated with the upsampled features, enriching the segmentation process with rich spatial information. This combination significantly enhanced the segmentation accuracy. Eventually, a 3×3 convolution filter was applied, followed by upsampling by a factor of 4 to generate the final segmentation prediction.

The framework of the proposed model is visualized in Figure 3. In the first segmentation stage, DLT-LV model extracts the LV chamber, the target area where the myocardial scar is likely present. During the second segmentation stage, the model generates a predicted scar tissue mask based on the fusing information from the first stage's output and the original image.
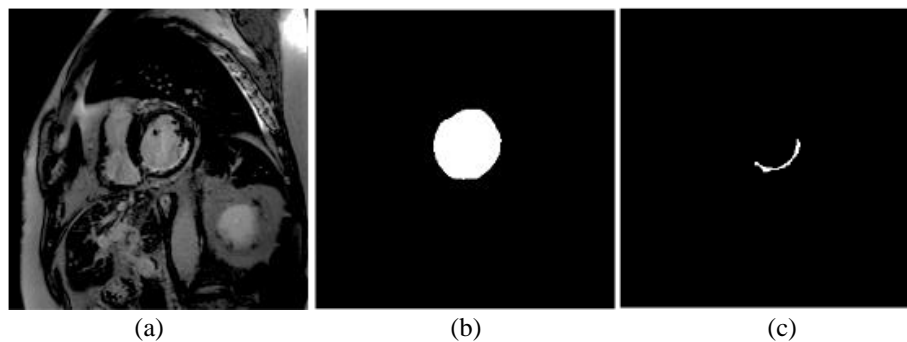

Figure 1. Example of the (a) short axis of LGE-CMR image, (b) manual LV chamber annotation by an expert radiologist and (c) infarcted scar tissue for validation purposes

2.2.1. Network backbone

The network backbone plays an essential role in feature extraction that captures relevant information from the input image. This study leveraged pre-trained architectures, renowned for their efficacy and efficiency, making it compatible with medical imaging tasks especially when handling limited training datasets. We adopted a dual-stage approach: Stage 1 employed MobileNetV2 [21], capitalizing on its lightweight design for swift feature extraction and LV chamber identification, minimizing computational burden for subsequent stages [22]. Stage 2 utilized ResNet50 [23], to extract finer details necessary for segmenting smaller scars [9], [24]–[26]. Both backbones were pre-trained on the ImageNet database and fine-tuned on their classification layers. They were then re-trained with our dataset to update the pre-trained weights for their specific segmentation task.
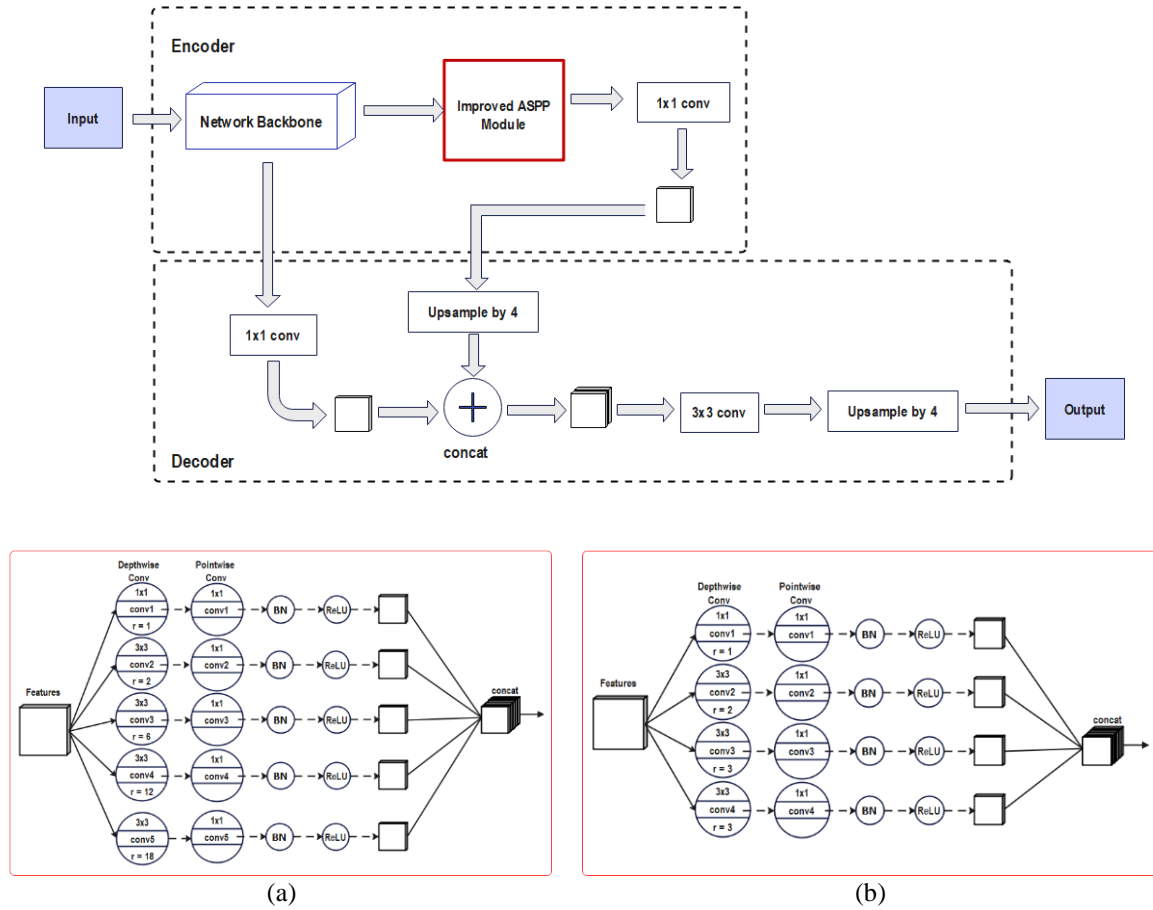
Figure 2. The encoder-decoder structure of the proposed model (a) improved ASPP module in LV segmentation model (DLT-LV) and (b) improved ASPP module in scar segmentation model. The 'r' denotes the atrous rate
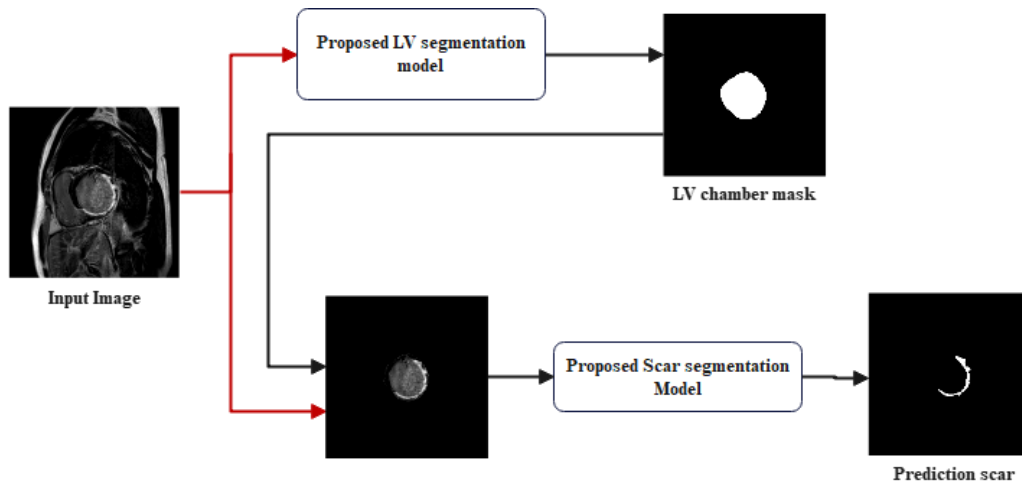

Figure 3. Framework of the proposed automatic dual-stage segmentation model

2.2.2. Imbalance dataset and loss function

Pixel ratio imbalance in the myocardial scar segmentation task was resolved by employing generalized Dice loss (GDL) function, a class-specific weighting approach, in all network models to control each class's contribution to the overall loss [27]. The GDL function is specifically suited for medical image segmentation tasks, as it addresses the challenge of imbalanced class distributions and varying region sizes. GDL is also designed to counter the influence of the background on the Dice score, allowing the model to

focus effectively on segmenting smaller regions. Smaller regions of higher weights were assigned to each class based on the inverse of its expected region area, thus enhancing their significance during the training process. GDL is computed as (1). The weighting factor w_k was calculated as the inverse of the expected region area for class k, aiding in effectively segmenting both large background and small regions in the medical images.

$$GDL(P,g)=1-2\,\frac{\sum_{k-1}^{n} w_k \sum_{i,j} P_{ijk} g_{ijk}}{\sum_{k-1}^{n} w_k \sum_{i,j} P_{ijk} + \sum_{i,j} g_{ijk}} \tag{1}$$

where P_{ijk} is the predicted probability of class k at pixel (i,j), g_{ijk} is the corresponding ground truth label (binary) of class k at pixel (i,j), w_k is the class-specific weight for class k, and n is the number of classes.

2.3. Evaluation metrics

Two standard metrics, the Dice coefficient and the Jaccard index, were used to assess the segmentation performance. The Dice coefficient determines the sum of the size of the predicted and ground truth regions, while the Jaccard index calculates the combined size of the predicted and ground truth regions as the union and takes their ratio. Mathematically, the Dice coefficient and Jaccard index are calculated using (2) and (3) based on the true positive (TP), false positive (FP), and false negative (FN) values.

$$Dice\ coefficient=\frac{2TP}{2TP+FP+FN} \tag{2}$$

$$Jaccard\ index=\frac{TP}{TP+FP+FN} \tag{3}$$

The mean Dice score was obtained by evaluating the model's segmentation performance across multiple images. The mean Dice score was chosen as the primary evaluation metric to be discussed in the result and discussion section. This decision was based on its higher sensitivity to small variances in the overlap and widespread application in medical image segmentation [28].

2.4. Algorithm implementation and performance analysis

The algorithm was implemented using MATLAB software version R2022b. In order to avoid the potential impact of hyperparameters, all experiments utilized the Adam optimizer [29] with a fixed learning rate of 0.001. The training process was conducted on a computer system equipped with an NVIDIA GeForce RTX 3070 GPU and 8 GB of RAM. To further evaluate the significance of the proposed framework, a comparative analysis was conducted against the baseline DeepLabV3+ architecture [19] with MobileNetV2 and ResNet50 backbone for both stages, respectively.

3. EXPERIMENTAL RESULTS AND DISCUSSION
3.1. Analysis of left ventricle chamber segmentation

Table 1 shows the experimental results comparing the proposed DLT-LV model's performance in first stage segmentation against two original DeepLabV3+ architecture as the baseline model. The first baseline model uses the same MobileNetV2 backbone as the proposed DLT-LV model, allowing for a direct comparison of the modified ASPP module's impact. The second baseline utilizes the more complex Xception backbone to assess the lightweight MobileNetV2's capability of achieving high accuracy. Overall, the proposed DLT-LV achieved an improved mean Dice score of 96.02% for the LV chamber class, surpassing both baseline DeepLabV3+ variants by 1.63% improvement over DeepLabV3+(Xception) and a 1.26% enhancement over DeepLabV3+ (MobileNetV2). Notably, the proposed model also achieved a superior Jaccard index of 93.15% for the LV chamber, further corroborating its ability to produce highly accurate segmentation masks that closely align with ground truth annotations. All models demonstrated exceptional performance with a high accuracy rate of over 99% for the background class. The proposed model requires only 6.9 million learnable parameters, a significant reduction compared to DeepLabV3+(Xception) with its 26.8 million parameters. This highlights the proposed backbone model's ability to deliver exceptional segmentation accuracy while maintaining a compact and efficient architecture, as a promising solution for medical imaging analysis in clinical settings with limited computational resources.

Figures 4 illustrate the effectiveness of the proposed DLT-LV model for segmenting the different scales in the LV chamber (apical, middle, and basal region) compared to two baseline networks. The arrow highlights areas where the segmentation outputs deviate from the ground truth. The images reveal the

segmentation output of automated segmentation overlay on the original image with 0.4 transparency. All networks demonstrated excellent segmentation coverage within the middle LV chamber yet encountered challenges in accurately segmenting the top basal and lowest apical area. Notably in these challenging areas, the segmentation output of the DLT-LV model may not achieve exact border delineation of the LV chamber that perfectly aligns as the ground truth, but it effectively captures all features within the region of interest. Hence, the proposed DLT-LV model exhibited a relatively improved segmentation in these challenging areas compared to both benchmark models.

Table 1. Comparison of the proposed model with baseline DeepLabV3+ model in LV chamber segmentation

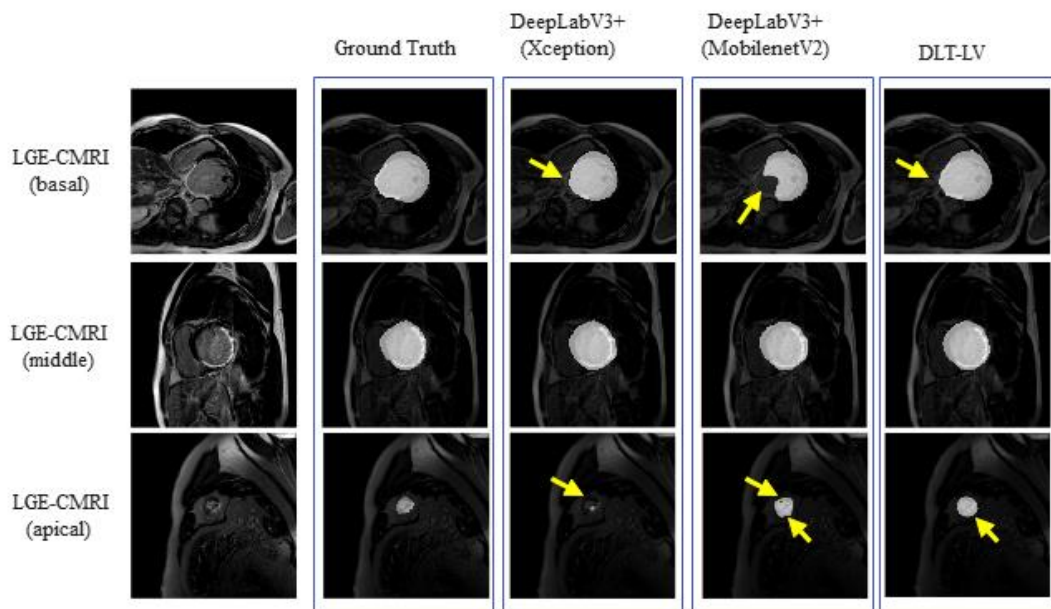| Network (backbone) First stage	Mean Dice (%)		Jaccard index (%)		Overall Dice score	Total learnable parameter/ Million
	LV chamber	Background	LV chamber	Background		
DeepLabV3+ (Xception)	94.39	99.81	92.06	99.62	97.10	26.8
DeepLabV3+ (MobileNetV2)	94.76	99.80	92.08	99.61	97.28	6.6
Proposed DLT-LV (MobileNetV2)	96.02	99.83	93.15	99.69	97.93	6.9

Figure 4. The first stage visual LV chamber segmentation results in lowest apical, middle, and basal region on LGE-CMR image and its ground truths

3.2. Analysis of scar segmentation

As shown in Table 2, two combination schemes of original DeepLabV3+(ResNet50) architecture model for scar segmentation in was compared with the proposed dual-stage model. The first scheme applied the baseline DeepLabV3+(MobileNetV2) model for LV chamber segmentation in the first stage and the second scheme used the proposed DLT-LV (MobileNetV2) for LV chamber segmentation in first stage. Across all network configurations, the combination models with the proposed DLT-LV model at the first stage consistently achieved higher scar Dice scores and Jaccard index compared to the baseline DeepLabV3+. This improvement scar Dice scores ranged from 3.72% for proposed DLT-LV with baseline DeepLabV3+ (ResNet50) in second stage and to 7.12% for our proposed dual-stage model, demonstrating the capability of DeeplabV3+ architecture in capturing scar features, particularly when used our proposed DLT-LV as the first stage LV chamber segmentation model. The proposed dual-stage using DeeplabV3+-based model achieved mean scar Dice scores of 68.01% and Jaccard index of 57.68% outperformed both baseline model showing the effectiveness of the improved ASPP module.

Table 2. Comparison of the proposed dual-stage model with original DeepLabV3+ architecture in myocardial scar segmentation

| Network (Backbone) | | Mean Dice (%) | | Jaccard index (%) | | Overall |
First stage	Second stage	Background	Scar	Background	Scar	Dice score
DeepLabV3+(MobileNetV2)	DeepLabV3+(ResNet50)	99.87	60.89	99.74	49.93	80.38
Proposed DLT-LV (MobileNetV2)	DeepLabV3+(ResNet50)	99.87	64.61	99.75	53.79	82.24
Proposed DLT-LV (MobileNetV2)	Proposed DeepLabV3+ (ResNet50)	99.88	68.01	99.76	57.68	83.95

3.3. Discussion

Compared to previous works performance as in Table 3, our proposed dual-stage model achieved better performance with a mean Dice score of 68.01%. Our model addresses the limitations of previous works by using end-to-end global segmentation approach, without cropping the region of interest. Furthermore, the dataset utilizes the entire slices range of LGE-CMR images from lowest epical and upper basal region making it more practical for real-scenario applications. Regardless, it is essential to acknowledge that the comparison with previous works may not be entirely reliable due to variations in datasets, which can significantly impact the overall results. Each dataset may exhibit different degrees of complexity and variations in imaging quality, influencing the performance of segmentation algorithms.

Table 3. Comparison of the proposed dual-stage model with related works in myocardial scar segmentation

Model		Dataset	Myocardial scar mean Dice score (%)
Moccia et al. [17]	-FCNNs	LGE (private)	55
Chen et al. [18]	-U-net	LGE (private)	67
Dan et al. [30]	-Deep Learning	LGE (private)+artificial LGE (GAN)	57
Our proposed dual stage model		LGE (private)	68.01

In the first stage segmentation, the DLT-LV model has demonstrated its efficacy as a reliable approach for segmenting the LV chamber with higher mean Dice score and Jaccard index above 96% and 93% respectively. We found that this proposed model is capable in handling variations in LV chamber size, particularly at the lowest epicardial and upper basal region. Despite the improvement achieved in the subsequent stage, delineating myocardial scar tissue from LGE-CMR images remains a challenging task, as evidenced by the mean Dice score still falling below 70%. This challenge arises from the inherent intricacy of the scar tissue, the variability in pixel intensities that complicate precise delineation, and the relatively small size of the infarcted scar compared to the background class. Although the GDL function addressed the imbalanced pixel distribution among the classes, it was only partially effective as it was unable to adequately handle the challenges posed by the hard sample problems arises from complex or ambiguous features in certain samples, causing difficulty to distinguish from other classes. Furthermore, such images may be rare, have unusual characteristics, or fall near the decision class boundary, making them challenging for the model to learn due to limited training data. As a result, certain scar regions posed significant difficulty in achieving accurate segmentation.

It is also critical to acknowledge some limitations of this study, which should be further investigated. Firstly, the generalization of the proposed model was only applied to a small dataset. Thus, further training and validation on larger and diverse datasets must be conducted using the proposed model. Additionally, the GDL was the only function utilized in this study. Hence, investigating diverse loss functions in handling the hard sample problem will be explored in our future research to improve the scar segmentation performance. Despite these limitations, the proposed dual-stage DeepLabV3+ model offers a valuable contribution to automated myocardial scar segmentation using LGE-CMR images, promising prospects for advancing cardiac image analysis in clinical practice. This research can be further used for myocardial infarction quantification diagnosis benefiting patients with cardiac diseases.

4. CONCLUSION

This study introduced a new automatic dual-stage DeepLabV3+-based model for myocardial scar tissue segmentation in short-axis LGE-CMR images. By leveraging the strengths of pretrained MobileNetV2 and ResNet50 as the network backbones and modified ASPP module with lower atrous dilated rates to optimize each specific task contributed to precise and reliable segmentation, leading to a Dice score of 96.02% for LV chamber segmentation and 68.01% for scar tissue extraction. Hence, the proposed dual-stage DeepLabV3+ based model demonstrated better performance, surpassing previous works in myocardial scar

segmentation in small dataset and has valuable contribution to myocardial scar segmentation, paving the way for enhanced clinical applications in cardiac image analysis.

REFERENCES

[1]   WHO, "Cardiovascular Diseases (CVDs)," *World Health Organization*. pp. 123–141, 2002, Accessed: Nov. 29, 2021. [Online]. Available: https://www.who.int/news-room/fact-sheets/detail/cardiovascular-diseases-(cvds).

[2]   W.-F. Khaw, Y. M. Chan, N. H. Nasaruddin, N. Alias, L. Tan, and S. S. Ganapathy, "Malaysian burden of disease: years of life lost due to premature deaths," *BMC Public Health*, vol. 23, no. 1, Jul. 2023, doi: 10.1186/s12889-023-16309-z.

[3]   B. Tasci, "Automated ischemic acute infarction detection using pre-trained CNN models' deep features," *Biomedical Signal Processing and Control*, vol. 82, p. 104603, Apr. 2023, doi: 10.1016/j.bspc.2023.104603.

[4]   M. Stuber and A. L. Baggish, "Acute myocardial injury in the COVID-HEART Study: Emphasizing scars while reassuring scares," *Circulation*, vol. 147, no. 5, pp. 375–377, Jan. 2023, doi: 10.1161/circulationaha.122.062508.

[5]   F. Li, W. Li, X. Gao, R. Liu, and B. Xiao, "Comprehensive information integration network for left atrium segmentation on LGE CMR images," *Biomedical Signal Processing and Control*, vol. 81, Art. no. 104537, Mar. 2023, doi: 10.1016/j.bspc.2022.104537.

[6]   A. M. West and C. M. Kramer, "Cardiovascular magnetic resonance imaging of myocardial infarction, viability, and cardiomyopathies," *Current Problems in Cardiology*, vol. 35, no. 4, pp. 176–220, Apr. 2010, doi: 10.1016/j.cpcardiol.2009.12.002.

[7]   J. Artico *et al.*, "Myocardial involvement after hospitalization for COVID-19 complicated by troponin elevation: A prospective, multicenter, observational study," *Circulation*, vol. 147, no. 5, pp. 364–374, Jan. 2023, doi: 10.1161/circulationaha.122.060632.

[8]   K. Raj Singh, A. Sharma, and G. Kumar Singh, "Attention-guided residual W-Net for supervised cardiac magnetic resonance imaging segmentation," *Biomedical Signal Processing and Control*, vol. 86, Art. no. 105177, Sep. 2023, doi: 10.1016/j.bspc.2023.105177.

[9]   M. Bal-Ghaoui, M. H. El Yousfi Alaoui, A. Jilbab, and A. Bourouhou, "U-Net transfer learning backbones for lesions segmentation in breast ultrasound images," *International Journal of Electrical and Computer Engineering (IJECE)*, vol. 13, no. 5, pp. 5747-5754, Oct. 2023, doi: 10.11591/ijece.v13i5.pp5747-5754.

[10] F. S. Khan, M. I. Abbasi, M. Khurram, M. N. Haji Mohd, and M. D. Khan, "Breast cancer histological images nuclei segmentation and optimized classification with deep learning," *International Journal of Electrical and Computer Engineering (IJECE)*, vol. 12, no. 4, pp. 4099-4110, Aug. 2022, doi: 10.11591/ijece.v12i4.pp4099-4110.

[11] M. F. Abdullah, S. N. Sulaiman, M. K. Osman, N. K. Abdul Karim, S. Setumin, and I. S. Isa, "A new procedure for lung region segmentation from computed tomography images," *International Journal of Electrical and Computer Engineering (IJECE)*, vol. 12, no. 5, pp. 4978-4987, Oct. 2022, doi: 10.11591/ijece.v12i5.pp4978-4987.

[12] C. Chen *et al.*, "Deep learning for cardiac image segmentation: A Review," *Frontiers in Cardiovascular Medicine*, vol. 7, Mar. 2020, doi: 10.3389/fcvm.2020.00025.

[13] Y. Liu, M. Zhang, Q. Zhan, D. Gu, and G. Liu, "Two-stage method for segmentation of the myocardial scars and edema on multi-sequence cardiac magnetic resonance," in *Lecture Notes in Computer Science*, Springer International Publishing, 2020, pp. 26–36.

[14] A. S. Fahmy, E. J. Rowin, R. H. Chan, W. J. Manning, M. S. Maron, and R. Nezafat, "Improved quantification of myocardium scar in late gadolinium enhancement images: Deep learning based image fusion approach," *Journal of Magnetic Resonance Imaging*, vol. 54, no. 1, pp. 303–312, Feb. 2021, doi: 10.1002/jmri.27555.

[15] X. Zhuang *et al.*, "Cardiac segmentation on late gadolinium enhancement MRI: A benchmark study from multi-sequence cardiac MR segmentation challenge," *Medical Image Analysis*, vol. 81, Art. no. 102528, Oct. 2022, doi: 10.1016/j.media.2022.102528.

[16] W. Li, L. Wang, F. Li, S. Qin, and B. Xiao, "Myocardial pathology segmentation of multi-modal cardiac MR images with a simple but efficient Siamese u-shaped network," *Biomedical Signal Processing and Control*, vol. 71, Art. no. 103174, Jan. 2022, doi: 10.1016/j.bspc.2021.103174.

[17] S. Moccia *et al.*, "Development and testing of a deep learning-based strategy for scar segmentation on CMR-LGE images," *Magnetic Resonance Materials in Physics, Biology and Medicine*, vol. 32, no. 2, pp. 187–195, Nov. 2018, doi: 10.1007/s10334-018-0718-4.

[18] Z. Chen *et al.*, "Automatic deep learning-based myocardial infarction segmentation from delayed enhancement MRI," *Computerized Medical Imaging and Graphics*, vol. 95, Art. no. 102014, Jan. 2022, doi: 10.1016/j.compmedimag.2021.102014.

[19] L.-C. Chen, Y. Zhu, G. Papandreou, F. Schroff, and H. Adam, "Encoder-decoder with atrous separable convolution for semantic image segmentation," in *Lecture Notes in Computer Science*, Springer International Publishing, 2018, pp. 833–851.

[20] J. Liu, M. Li, Y. Luo, S. Yang, W. Li, and Y. Bi, "Alzheimer's disease detection using depthwise separable convolutional neural networks," *Computer Methods and Programs in Biomedicine*, vol. 203, Art. no. 106032, May 2021, doi: 10.1016/j.cmpb.2021.106032.

[21] M. Sandler, M. Zhu, A. Zhmoginov, and C. V Mar, "MobileNetV2: Inverted residuals and linear bottlenecks," in *2018 IEEE/CVF*

Conference on Computer Vision and Pattern Recognition, Salt Lake City, UT, USA, 2018, pp. 4510-4520, doi: 10.1109/CVPR.2018.00474.

[22] H. Liu, Z. Xu, and B. Xu, "Research on improved DeepLabv3+ image Semantic Segmentation algorithm," in *Proceedings of the 7th International Conference on Control Engineering and Artificial Intelligence, CCEAI '23*, Jan. 2023, pp. 137–142, doi: 10.1145/3580219.3580244.

[23] K. He, X. Zhang, S. Ren, and J. Sun, "Deep residual learning for image recognition," in *2016 IEEE Conference on Computer Vision and Pattern Recognition (CVPR)*, Jun. 2016, pp. 770–778, doi: 10.1109/CVPR.2016.90.

[24] H. Cui, Y. Li, L. Jiang, Y. Wang, Y. Xia, and Y. Zhang, "Improving myocardial pathology segmentation with U-Net++ and EfficientSeg from multi-sequence cardiac magnetic resonance images," *Computers in Biology and Medicine*, vol. 151, Art. no. 106218, Dec. 2022, doi: 10.1016/j.compbiomed.2022.106218.

[25] D. R. P. R. M. Lustermans, S. Amirrajab, M. Veta, M. Breeuwer, and C. M. Scannell, "Optimized automated cardiac MR scar quantification with GAN-based data augmentation," *Computer Methods and Programs in Biomedicine*, vol. 226, Art. no. 107116, Nov. 2022, doi: 10.1016/j.cmpb.2022.107116.

[26] D. M. Papetti *et al.*, "An accurate and time-efficient deep learning-based system for automated segmentation and reporting of cardiac magnetic resonance-detected ischemic scar," *Computer Methods and Programs in Biomedicine*, vol. 229, Art. no. 107321, Feb. 2023, doi: 10.1016/j.cmpb.2022.107321.

[27] C. H. Sudre, W. Li, T. Vercauteren, S. Ourselin, and M. Jorge Cardoso, "Generalised Dice overlap as a deep learning loss function for highly unbalanced segmentations," in *Lecture Notes in Computer Science*, Springer International Publishing, 2017, pp. 240–248.

[28] D. Müller, I. Soto-Rey, and F. Kramer, "Towards a guideline for evaluation metrics in medical image segmentation," *BMC Research Notes*, vol. 15, no. 1, Jun. 2022, doi: 10.1186/s13104-022-06096-y.

[29] A. Kumar, S. Sarkar, and C. Pradhan, "Malaria disease detection using CNN technique with SGD, RMSprop and ADAM optimizers," in *Deep Learning Techniques for Biomedical and Health Informatics*, Springer International Publishing, 2019, pp. 211–230.

[30] D. M. Popescu *et al.*, "Anatomically informed deep learning on contrast-enhanced cardiac magnetic resonance imaging for scar segmentation and clinical feature extraction," *Cardiovascular Digital Health Journal*, vol. 3, no. 1, pp. 2–13, Feb. 2022, doi: 10.1016/j.cvdhj.2021.11.007.

BIOGRAPHIES OF AUTHORS

Dayang Suhaida Awang Damit received her MSc in electronic design from the School of Electrical and Electronics Engineering, Universiti Sains Malaysia in 2010. Currently, she is doing her Ph.D. in biomedical engineering at Universiti Teknologi MARA, Malaysia. Her research interests include image processing, artificial intelligence and wireless communication. She can be contacted at email: dayang671@uitm.edu.my.

Siti Noraini Sulaiman obtained her Ph.D. degree in (Imaging) from the School of Electrical and Electronics Engineering, Universiti Sains Malaysia in 2012. Currently, she is an associate professor at the Faculty of Electrical Engineering, Universiti Teknologi MARA, Penang Campus, Malaysia. She is also now attached as the chair of Advanced Rehabilitation Engineering in Diagnostic and Monitoring Research Group (AREDiM) and the deputy chair of Advanced Control System and Computing Research Group (ACSCRG), Universiti Teknologi MARA, Penang Campus in Permatang Pauh, Penang, Malaysia. Her main research interest is biomedical engineering focusing on image filtering, image clustering and algorithms for image processing. She can be contacted at email: sitinoraini@uitm.edu.my.

Muhammad Khusairi Osman obtained his B.Eng degree in electrical and electronic engineering in 2000 and MSc in electrical and electronic engineering in 2004 from Universiti Sains Malaysia. In 2014, he obtained his Ph.D. in medical electronic engineering from Universiti Malaysia Perlis (UniMAP), Malaysia. He is currently a senior lecturer at Faculty of Electrical Engineering, Universiti Teknologi MARA (UiTM), Malaysia. His research interest is in image processing, pattern recognition and artificial intelligence. He can be contacted at email: khusairi@uitm.edu.my.

Noor Khairiah A. Karim 🆔 ⑧ SC ⟲ received her bachelor degree in medicine, bachelor degree in surgery (MBBS), and master of radiology (MRad) from the University of Malaya, Malaysia. She then obtained her Fellowship in Cardiac Imaging from the National Heart Center Singapore. She is currently a senior medical lecturer of the regenerative medicine cluster, and a consultant radiologist at the Advanced Medical and Dental Institute, Universiti Sains Malaysia. Her current research areas include medical image processing and analysis with a special interest in cardiac, breast and brain imaging. She can be contacted at email: drkhairiah@usm.my.

Samsul Setumin 🆔 ⑧ SC ⟲ received the B.Eng. degree (Hons.) in electronic engineering from the University of Surrey, in 2006, and the M.Eng. degree in electrical-electronic and telecommunication from the Universiti Teknologi Malaysia, in 2009. He obtained his Ph.D. degree from Universiti Sains Malaysia in 2019 in the imaging field. Since 2010, he has been a lecturer with the Universiti Teknologi MARA, Malaysia. He was a test engineer with Agilent Technologies (M) Sdn. Bhd., and Intel Microelectronics (M) Sdn. Bhd., for a period of one year. His research interests include computer vision, image processing, pattern recognition, and embedded system design. He can be contacted at email: samsuls@uitm.edu.my.